

A Gas-Surface Interaction Model for Spatial and Time-Dependent Friction Coefficient in Reciprocating Contacts: Applications to Near-Frictionless Carbon

P. L. Dickrell
W. G. Sawyer¹

Department of Mechanical and Aerospace
Engineering,
University of Florida,
Gainesville, FL 32611

J. A. Heimberg
I. L. Singer
K. J. Wahl

Naval Research Laboratory,
Tribology Section Code 6176,
Washington, DC 20375

A. Erdemir
Argonne National Laboratory,
Energy Technology Division,
Argonne, IL 60439

A closed-form time- and position-dependent model for coverage, based on the adsorption of environmental contaminants and their removal through the pin contact, is developed for reciprocating contacts. The model employs an adsorption fraction and removal ratio to formulate a series expression for the entering coverage at any cycle and location on the wear track. A closed-form solution to the series expression is presented and compared to other coverage models developed for steady-state coverage for pin-on-disk contacts, reciprocating contacts, or the time-dependent center-point model for reciprocating contacts. The friction coefficient is based on the average coverage under the pin contact. The model is compared to position- and time-dependent data collected on near-frictionless carbon self-mated contacts on a reciprocating tribometer in a nitrogen atmosphere. There are many similarities between the model curves and the data, both in magnitude and trends. No new curve fitting was performed in this paper, with all needed parameters coming from previous models of average friction coefficient behavior. [DOI: 10.1115/1.1829719]

Introduction

Diamondlike carbon (DLC) films are of tribological interest due to their low friction, low wear rate, high hardness, and chemical inertness [1,2]. A class of diamondlike carbon coatings termed near-frictionless carbon (NFC), developed at Argonne National Laboratory, has been shown to sustain superlow coefficients of friction ($\mu < 0.003$) and wear rates ($K < 3^{-10} \text{ mm}^3/\text{Nm}$) in self-mated contacts [3]. Details on the preparation and characteristics of the films have been addressed in other literature [4]. The tribological behavior of these films is sensitive to the environment, only realizing their low friction coefficient and wear rate in inert, dry, or vacuum environments [3,5–8]. The NFC films used in this study have a high hydrogen content. When gaseous water is added to the environment, the friction coefficient in NFC self-mated contacts rises [8], suggesting a gas-surface interaction where water molecules disrupt the low friction of the NFC pair. Velocity-dependent friction coefficients of these films in nitrogen atmospheres were measured by Heimberg et al. [7]. They hypothesized that the velocity dependence was due to a gas-surface interaction that had longer times to affect the film at slower sliding speeds. This hypothesis was further supported by experiments that varied exposure time under constant sliding speeds using periods of dwell at the reversal locations. These tests showed a clear dependence on exposure time as opposed to velocity.

Environment-surface interaction models have been created by many research groups in an attempt to describe friction coefficient variations in tribological experiments. To the authors' knowledge, the first modeling of this in tribology is the work of Rowe [9], who used the Langmuir adsorption model [10] to describe the

wear in boundary lubrication. Gas-surface interactions were reported in 1957 by Bowden and Rowe [11] to describe the lubrication of molybdenum in hydrogen disulfide gases, but were not modeled. Blanchet et al. [12] included both deposition and removal rates in a model developed to study transitions from adequate to inadequate lubrication in vapor phase lubrication; this model was based on balancing the rates of layer formation and removal, but was not fractional (friction was predicted to be either low or high in the adequate or inadequate regime, respectively). A time-dependent coverage model, without removal, was proposed by Zaidi et al. [13] to describe gas interactions with carbon surfaces. The interaction kinetics used followed the work of Elovitch [14]. Models that predict steady-state friction coefficients for pin-on-disk contacts and combined rolling and sliding contacts [15] were developed by applying the competitive rate model of Blanchet et al. [12] with fractional surface adsorption [10] and fractional removal [16]. This effort was then extended by Dickrell et al. [17] for the pin-on-disk (or midpoint of a reciprocating path) case to include the transient effects. The model was developed by recursively applying fractional adsorption and fractional removal during each contact. The derived closed-form solution predicted fractional surface coverage for both transient and steady-state conditions, matching previously derived steady-state models exactly. Table 1 shows modeling nomenclature, and Fig. 1 shows the fit of this model [17] to the average (per cycle) frictional data from Heimberg et al. [7], which were collected on NFC in a nitrogen gas environment using a reciprocating tribometer. As previously discussed, the speed-dependent effects were hypothesized to be related to gas-surface interactions.

Modeling gas-surface interactions in reciprocating contacts poses significant challenges at locations other than the midpoint. This was recently addressed in a model by Sawyer and Dickrell [18], which looked at the exposure time for forward and reverse sliding directions as a function of position along the track, sliding

¹Corresponding Author: W. Gregory Sawyer, Department of Mechanical and Aerospace Engineering, University of Florida, Gainesville, FL 32611, phone: (352) 392-8488, fax: (352) 392-1071, email: wgsawyer@ufl.edu

Manuscript received March 2, 2004; revision received July 26, 2004. Review conducted by: M. Fillon.

Table 1 Parameters used in model derivation

Parameter	Definition
α	adsorption fraction
subscript f	denotes "forward" direction
λ	removal ratio (θ_{out}/θ_{in})
μ_0	friction coefficient of nascent surface
μ_1	friction coefficient of covered surface
n	cycle number
ν	deposition constant
P	partial pressure
$1 - \theta$	nascent surface area fraction
subscript r	denotes "reverse" direction
T	cycle time for a single cycle (forward and reverse)
t	time between contact for a specific wear track location
V	velocity

speed, and dwell times. The model coupled fractional adsorption with fractional removal to predict steady-state coverage at different track locations.

This current modeling activity aims to combine the approaches of the previous time-dependent coverage model [17] with the spatially dependent steady-state model of reciprocating contacts [18] to develop a closed-form time and position-dependent coverage model in a reciprocating contact. Friction coefficients computed from the model will then be compared to position-dependent friction coefficients from NFC coatings tested at various speeds in dry N_2 . The friction data were collected by Heimberg et al. [7], but only the averaged data were presented in [7]. Here, the position-dependent data are reported and analyzed.

Modeling

In reciprocating tribometry, every location on the wear track comes in and out of contact with the pin moving either forward (subscript f) or reverse (subscript r); it makes no difference whether the pin or the counterface is moving for the purposes of modeling, which uses a counterface-attached coordinate system for the derivation. The amount of time a particular location is exposed to the environment is a function of its location, the overall path length, and sliding speed of the pin, which is assumed to be constant along the track length. The increase in coverage at a particular location is a function of the surface area fraction θ when the pin last exposed the counterface at that position and the amount of time $t_{(f,r)}$ that the location was exposed to the environment before the pin returned. In this modeling, the surface area fraction θ is always between 0 (completely nascent surface) and 1 (completely interacted/covered surface). One item to note is the distinction between the forward t_f and reverse t_r exposure times. For any given position along the wear track there exists unique values for t_f and t_r ; only at the midpoint does $t_f=t_r$. The total cycle time T is defined as the sum of the forward and reverse portions of the cycle motion, $T=t_f+t_r$. Speed dependence of the friction coefficient is attributed to a change in exposure time between contacts, the faster the sliding speed, the less time between pin contacts [lower values of $t_{(f,r)}$]. Tables 1 and 2 and Fig. 2 show the nomenclature, equations, and schematic used for this position and time-dependent modeling.

The modeling initiates with each position along the track having $\theta=0$ coverage for the first forward pass. On the first reverse pass, the pin has traveled to the end of the wear track and back to the position of interest. During this time the reverse adsorption

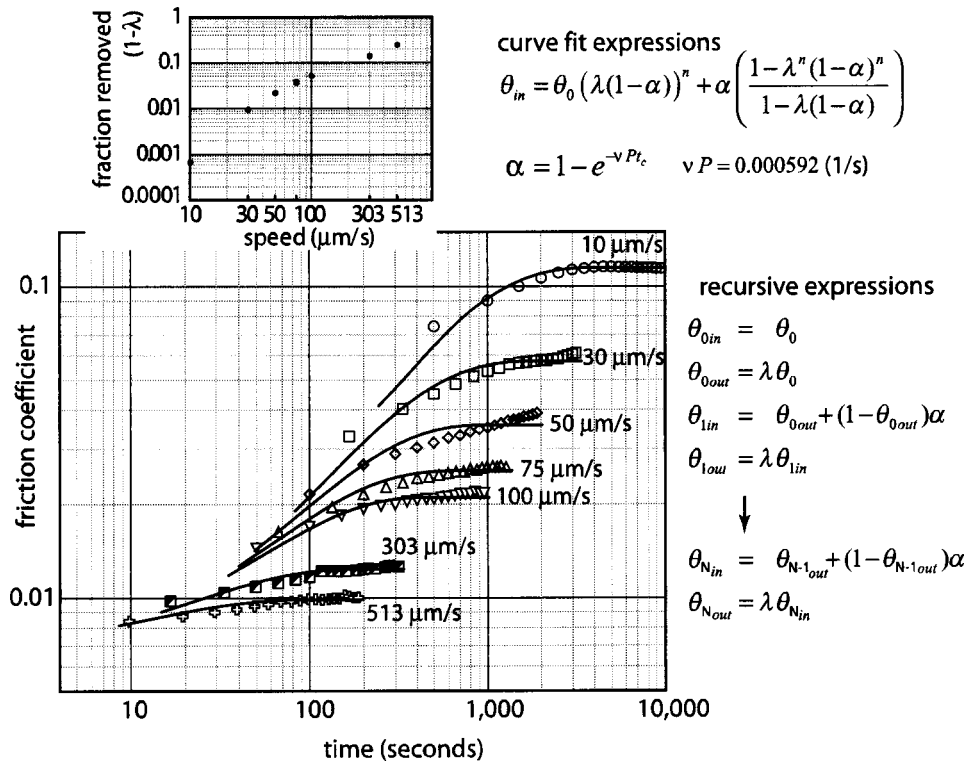


Fig. 1 Recursive relations used in the derivation of the midpoint model. A closed-form expression for entering coverage for any cycle n ($\theta_{n,in}$) is expressed as a function of initial coverage θ_0 , removal ratio λ , and adsorption coefficient α . Model line fits [17] are shown against averaged friction data collected by Heimberg et al. [7]. The adsorption fraction was found using Langmuir adsorption, where νP is an adsorption rate and t_c is the cycle time between the pin passes at the midpoint of the track. The values of νP and λ from this figure are used in the application of the positional and time-dependent model.

Table 2 Model expressions of coverage for the first two complete cycles of sliding. Equations are expressed for the inlet (subscript *in*) and outlet (subscript *out*) of the pin contact for each forward (subscript *f*) or reverse (subscript *r*) motion of sliding during a cycle.

1	f	in	$\theta_{f1in} = 0$	\rightarrow	0
		out	$\theta_{f1out} = \lambda(\theta_{f1in})$	\rightarrow	0
	r	in	$\theta_{r1in} = \theta_{f1out} + \alpha_r(1 - \theta_{f1out})$	\rightarrow	α_r
		out	$\theta_{r1out} = \lambda(\theta_{r1in})$	\rightarrow	$\lambda\alpha_r$
2	f	in	$\theta_{f2in} = \theta_{r1out} + \alpha_f(1 - \theta_{r1out})$	\rightarrow	$\lambda\alpha_r + \alpha_f(1 - \lambda\alpha_r)$
		out	$\theta_{f2out} = \lambda(\theta_{f2in})$	\rightarrow	$\lambda(\lambda\alpha_r + \alpha_f(1 - \lambda\alpha_r))$
	r	in	$\theta_{r2in} = \theta_{f2out} + \alpha_r(1 - \theta_{f2out})$	\rightarrow	$\lambda(\lambda\alpha_r + \alpha_f(1 - \lambda\alpha_r)) + \alpha_r(1 - \lambda(\lambda\alpha_r + \alpha_f(1 - \lambda\alpha_r)))$
		out	$\theta_{r2out} = \lambda(\theta_{r2in})$	\rightarrow	$\lambda \left(\begin{array}{l} \lambda(\lambda\alpha_r + \alpha_f(1 - \lambda\alpha_r)) + \\ \alpha_r(1 - \lambda(\lambda\alpha_r + \alpha_f(1 - \lambda\alpha_r))) \end{array} \right)$

fraction α_r acts on the nascent portion of the surface from the previous pass ($1 - \theta_{f,out}$), giving an entering coverage $\theta_{r,in}$ of the form $\theta_{(r,f),in} = \theta_{(f,r),out} + [1 - \theta_{(f,r),out}]\alpha_{(r,f)}$. This process continues, forward-reverse-forward-reverse, . . . , as illustrated in Fig. 2. The change in coverage that occurs when the pin rides over a particular location [$\theta_{(f,r),in} - \theta_{(f,r),out}$] follows a model for the frac-

tional removal of films proposed by Blanchet and Sawyer [16] and is of the form $\theta_{(f,r),out} = \lambda\theta_{(f,r),in}$, where λ is a removal ratio between $\lambda = 0$ (complete removal) and $\lambda = 1$ (no removal).

For consecutive forward and reverse passes, the difference in entering coverage is given in Table 3 for the first 4 cycles. The change in entering coverage is defined as $\Delta\theta_N = \theta_{N+1} - \theta_N$ for

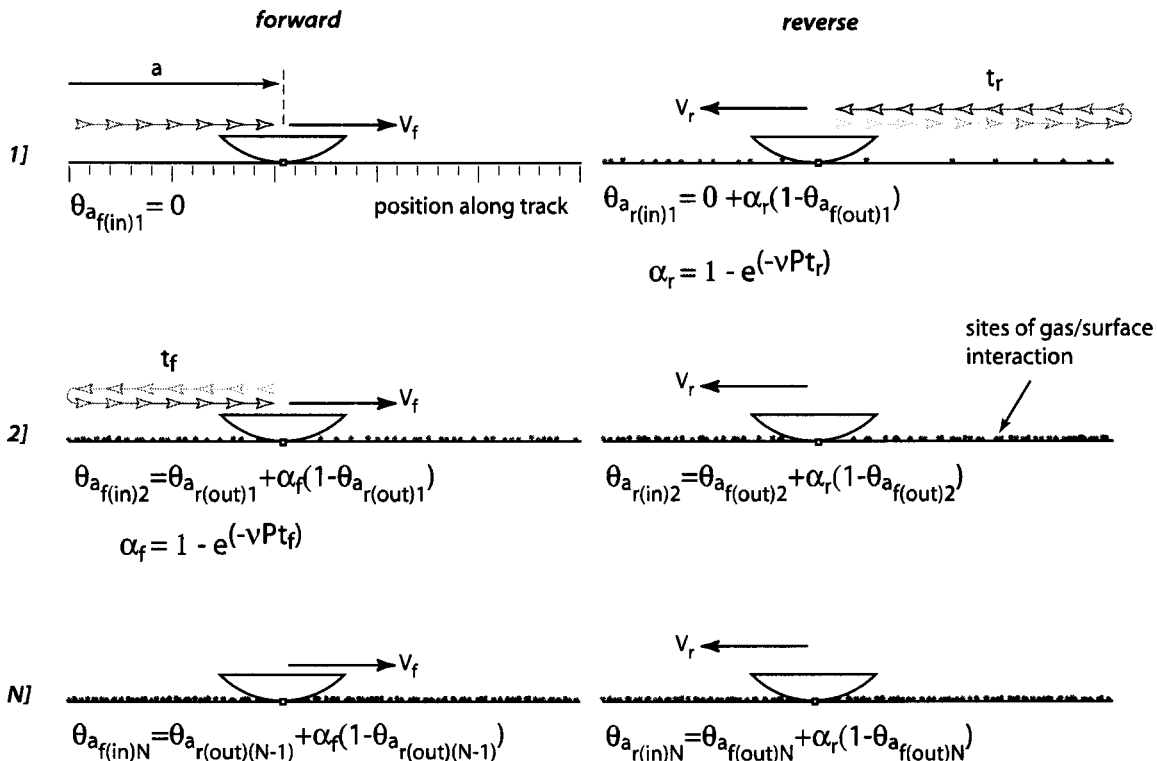


Fig. 2 Model schematic for position *a*. The times between contact when moving forward or reverse are t_f and t_r , respectively. The adsorption fractions for the forward and reverse contacts are α_f and α_r , respectively. Recursive equations are given for any cycle *N*.

Table 3 Differences of the entering coverage (forward or reverse) $\Delta\theta_{(f,r)N}$ between cycle $N+1$ and N . A pattern emerges from the equations leading to a closed-form expression for the change in coverage for any cycle N .

forward	reverse
$\Delta\theta_{f1} = (\alpha_r\lambda + \alpha_f - \alpha_f\alpha_r\lambda)$	$\Delta\theta_{r1} = \lambda(1 - \alpha_r)\Delta\theta_{f1}$
$\Delta\theta_{f2} = \lambda^2(1 - \alpha_f)(1 - \alpha_r)\Delta\theta_{f1}$	$\Delta\theta_{r2} = \lambda^3(1 - \alpha_f)(1 - \alpha_r)^2\Delta\theta_{f1}$
$\Delta\theta_{f3} = \lambda^4(1 - \alpha_f)^2(1 - \alpha_r)^2\Delta\theta_{f1}$	$\Delta\theta_{r3} = \lambda^5(1 - \alpha_f)^2(1 - \alpha_r)^3\Delta\theta_{f1}$
$\Delta\theta_{f4} = \lambda^6(1 - \alpha_f)^3(1 - \alpha_r)^3\Delta\theta_{f1}$	$\Delta\theta_{r4} = \lambda^7(1 - \alpha_f)^3(1 - \alpha_r)^4\Delta\theta_{f1}$
$\Delta\theta_{fN} = \lambda^{(2N-2)}(1 - \alpha_f)^{(N-1)}(1 - \alpha_r)^{(N-1)}\Delta\theta_{f1}$	$\Delta\theta_{rN} = \lambda^{(2N-1)}(1 - \alpha_f)^{(N-1)}(1 - \alpha_r)^N\Delta\theta_{f1}$

any cycle N , where the subscript N is understood to mean N_{in} . The patterns for the differences in entering coverage for forward and reverse passes in terms of cycle number, removal ratio λ , and the forward and reverse adsorption fractions α_f and α_r are given in Eqs. (1) and (2), respectively,

$$\Delta\theta_{fN} = \lambda^{2N-2}(1 - \alpha_f)^{N-1}(1 - \alpha_r)^{N-1}(\alpha_r\lambda + \alpha_f - \alpha_f\alpha_r\lambda) \quad (1)$$

$$\Delta\theta_{rN} = \lambda^{2N-1}(1 - \alpha_f)^{N-1}(1 - \alpha_r)^N(\alpha_r\lambda + \alpha_f - \alpha_f\alpha_r\lambda) \quad (2)$$

The coverage entering the pin contact for forward or reverse travel for any cycle (n) is the coverage entering the first cycle in that direction plus the sum of the differences in coverage up to that cycle (n), as given by Eq. (3).

$$\theta_{(f,r)n} = \theta_{(f,r)1} + \sum_{N=1}^n \Delta\theta_{(f,r)N} \quad (3)$$

Fortunately, there are closed-form solutions to the summations in Eq. (3), and the entering coverage for any cycle with the pin moving either forward or reverse is given in Eqs. (4) and (5), respectively.

$$\theta_{fn} = \frac{c(1 - g^{(n-1)})}{1 - g} \quad (4)$$

$$\theta_{rn} = \frac{b - cdg^{n-1}}{1 - g} \quad (5)$$

The variables (c , g , b , and d) are given in Table 4. The adsorption fractions can be expressed in a more traditional Langmuir form similar to previous models as given by Eqs. (6) and (7) for the forward and reverse cases, respectively.

$$\alpha_f = 1 - e^{-\nu Pt_f} \quad (6)$$

$$\alpha_r = 1 - e^{-\nu Pt_r} \quad (7)$$

The adsorption fractions are a function of the deposition constant ν , the partial pressure of the gas P , and the exposure time in the forward or reverse directions t_f, t_r . The only difference between the forward and reverse adsorption coefficients concerns the exposure time in the direction of travel t_f and t_r . Each position along the track has a unique value for t_f and t_r ; only at the midpoint of the track does $t_f = t_r$. The coefficients ν and P are constants for each experiment and are taken from the time-dependent curve fits reported in Ref. [17]. Following the work of Langmuir, these deposition constants are not spatially or time-dependent for a gaseous environment that is compositionally and thermally steady. Equations (8) and (9) give the closed-form expressions in a form similar to the position-dependent steady-state equations for reciprocating motion published in [18], where $T = t_f + t_r$.

$$\theta_{fn} = [1 - (1 - \lambda)e^{-\nu Pt_f} - \lambda e^{-\nu PT}] \frac{[1 - (\lambda^2 e^{-\nu PT})^{n-1}]}{[1 - \lambda^2 e^{-\nu PT}]} \quad (8)$$

$$\theta_{rn} = [1 - (1 - \lambda)e^{-\nu Pt_r} - \lambda e^{-\nu PT}] \frac{[\lambda e^{-\nu Pt_r} - e^{-\nu PT}(1 - \lambda + \lambda^2 e^{-\nu Pt_r})][\lambda^2 e^{-\nu PT}]^{n-1}}{[1 - \lambda^2 e^{-\nu PT}]} \quad (9)$$

The first check for the validity of Eqs. (8) and (9), which are spatially dependent (through t_f and t_r values) and time dependent (through the cycle number n), was to evaluate the limit of these functions as $n \rightarrow \infty$ and compare this to the previously developed steady-state expressions, which were created by balancing the deposition and removal rates at steady state. As expected, Eqs. (8) and (9) are identical to the steady-state equations published earlier [18]. The second check was to verify that this model matched the time-dependent model developed for the midpoint [17] when $t_f = t_r$. The final verification step was to take the limit of the model

Table 4 Expressions for the variables (c , g , b , and d) used in Eqs. (4) and (5). All variables are expressed in terms of the forward or reverse adsorption coefficient α_f, α_r and the removal ratio λ .

c	$\lambda\alpha_r(1 - \alpha_f) + \alpha_f$	$\lambda(1 - e^{-\nu Pt_r})e^{-\nu Pt_f} + (1 - e^{-\nu Pt_f})$
g	$(1 - \alpha_f)(1 - \alpha_r)\lambda^2$	$e^{-\nu Pt_f} e^{-\nu Pt_r} \lambda^2$
b	$\lambda\alpha_f(1 - \alpha_r) + \alpha_r$	$\lambda(1 - e^{-\nu Pt_f})e^{-\nu Pt_r} + (1 - e^{-\nu Pt_r})$
d	$\lambda(1 - \alpha_r)$	$\lambda e^{-\nu Pt_r}$

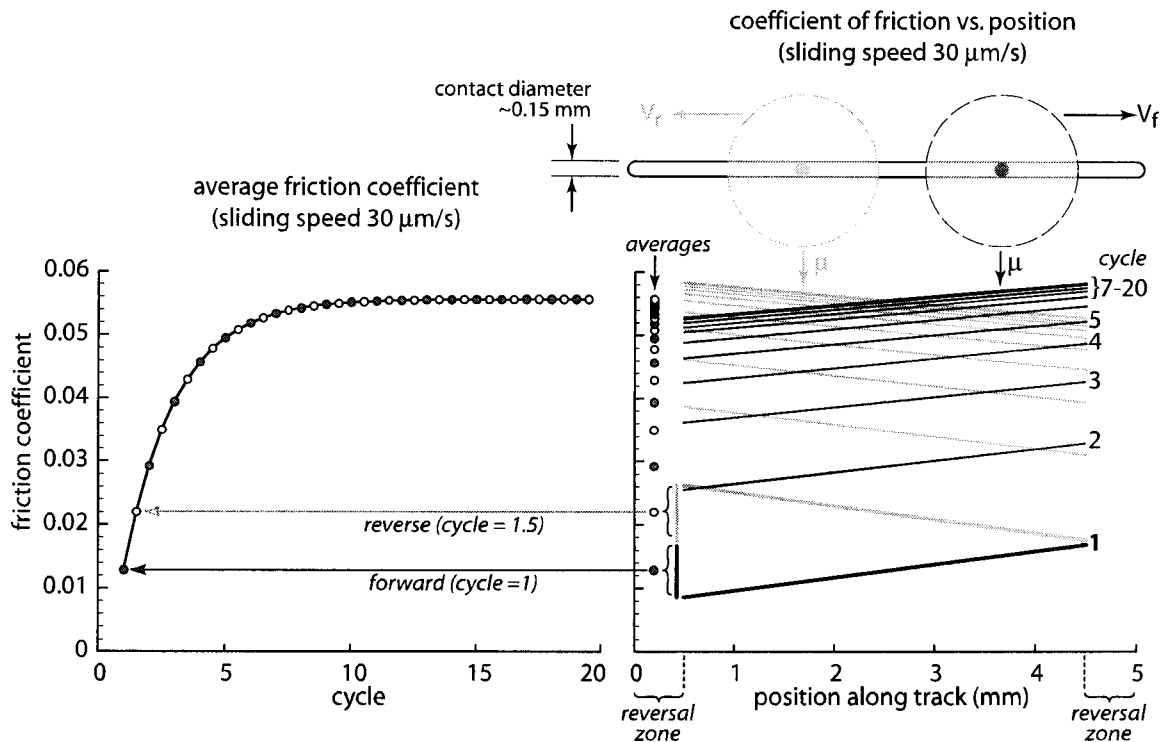


Fig. 3 Comparison of the midpoint model [17] (left) to the positional model (right) for a single sliding speed. The midpoint value at each forward or reverse pass corresponds well with the mean values because the trend is nearly perfectly linear in friction coefficient versus position. All model parameters are given in Fig. 1.

as $n \rightarrow \infty$ when $t_f = t_r$ and compare this to the steady-state pin-on-disk model [15], which was again developed by balancing the deposition and removal rates at steady state. In all of these cases, the model was able to be expressed in an equivalent form to the previously developed models. Fig. 3 shows the progression of the time- and position-dependent results of the model derived here and compared the average friction coefficient of the model to the time-dependent predictions of the midpoint reported in [17] using the same parameters.

To predict friction coefficients at specific pin locations, the average coverage within the contact $\bar{\theta}$ is calculated according to Ref. [16]. The friction coefficient μ is then calculated using the linear rule-of-mixtures [Eq. (10)] with μ_0 and μ_1 being the friction coefficients for the nascent surface and coverage, respectively

$$\mu = \mu_0 + \bar{\theta}(\mu_1 - \mu_0) \quad (10)$$

Experimental values for μ_0 and μ_1 are obtained in the case of NFC films by using the lowest μ_0 and highest μ_1 friction coefficients realized in the self-mated series of tests in dry nitrogen [7]. The values for μ_0 and μ_1 were also left as free parameters in model fits performed in [17], but the fit values did not vary substantially from the experimentally obtained values, so the experimental values are used.

Results and Discussion

The results of Heimberg et al. [7] on NFC sliding couples demonstrated that achieving superlow friction coefficients ($\mu < 0.01$) required that the NFC versus NFC interface be “wiped” frequently in a relatively moisture-free atmosphere (dry N_2). In this friction regime, as shown in both low-speed sliding tests and time-delayed high-speed sliding tests, the friction coefficient rose after each cycle of sliding, as predicted by the Elovitch model [7] and the Langmuir model [17]. The latter model shows that when the “wiping” rate is lower than the gas-surface interactions, the fric-

tion coefficient rises in proportion to the coverage. Figure 1 shows fits to the data in [7] using the model discussed in detail in [17].

The present model of spatially resolved friction behavior, however, provides a far more detailed picture of the competitive rates of Langmuir adsorption and fractional removal, which can be tested against NFC versus NFC data. During the experiments reported in [7], friction coefficient versus pin position data were taken. Figures 4 and 5 present the position- and cycle-dependent friction data and the presently derived model. The model curves in Figs. 4 and 5 use the parameters (νP , λ , μ_0 , and μ_1) determined from the time-averaged modeling [17], and no further curve fitting was performed.

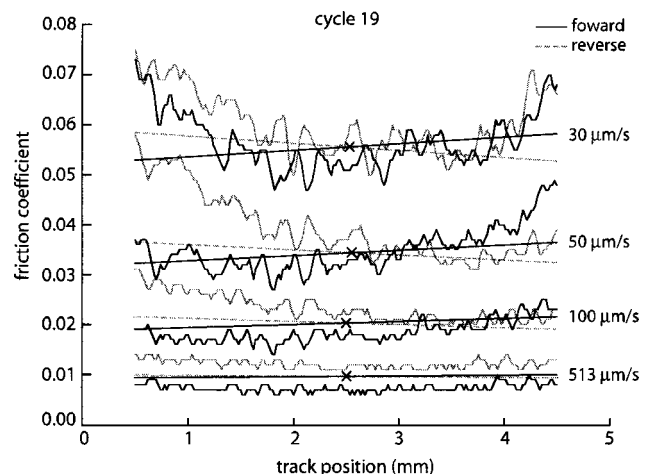


Fig. 4 Model comparisons to friction coefficient data for cycle 19/20 at multiple sliding speeds. All model parameters are given in Fig. 1.

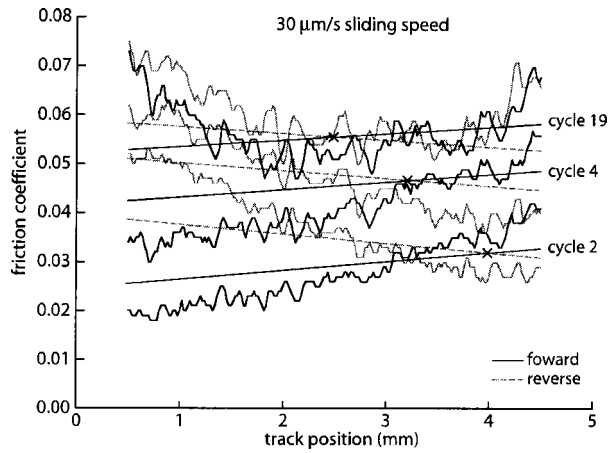


Fig. 5 Model comparisons to friction coefficient data from multiple cycles at a 30 $\mu\text{m/s}$ sliding speed. All model parameters are given in Fig. 1.

Figure 4 shows the model curves and data along the reciprocating length for cycle 19/20 under multiple sliding speeds (this condition was assumed to be nearly steady state). Figure 5 shows the model curves and data for multiple cycles during a single sliding speed. The data at the first and last 0.5 mm of track length were discarded due to the reversal zones, as discussed in [18]. The X marks in Figs. 4 and 5 correspond to the crossing points in the model, where the friction coefficient was the same in the forward and reverse motion directions for a specific cycle; at steady state this is at the midpoint.

There are similarities between the model curves and the data. First, the model tracks the midpoint friction coefficient data well. Second, the crossing point of the friction coefficient between the forward and reverse directions of motion for a given cycle occurs in similar locations along the track in both the model and data. In Fig. 4, the crossing points are located at approximately the midpoint of the track, when the model has reached steady state for multiple sliding speeds. As shown in Fig. 5, the crossing point for a single sliding speed progresses from the extremity of the wear track toward the midpoint as the friction coefficient progresses toward steady state.

In the low friction regime ($\mu < 0.05$), both the model curves and the data show nearly linear variations in friction coefficient versus track position, with a higher friction coefficient being found at the end of a cycle and lower friction coefficient at the beginning. Additionally, friction coefficients at a position on the track after the crossing point during forward motion are higher than the values at the same position after the turn around, during reverse motion. This difference in friction coefficient is due to the fact that for a specific track position past the midpoint, the exposure time between pin contacts is longer in the forward than in the reverse direction of travel, and the removal ratio is less than unity. Longer exposure time to the environment allows more adsorption and/or interaction to occur, resulting in a higher coverage and friction coefficient.

The linear variation of the model curves is surprising given that the surface coverage expressions have exponential dependencies. The forward-direction-entering coverage expression given in Eq. (4) is examined to illustrate why the model curves appear linear. Cycle dependence enters through the g^n in Eq. (4). Position dependence occurs in the c of the expression. From Table 3, $c = \lambda(1 - e^{-\nu P t_f})e^{-\nu P t_f} + (1 - e^{-\nu P t_f})$, which can also be written as $c = 1 - (1 - \lambda)e^{-\nu P t_f} - \lambda e^{-\nu P T}$. The only term that is track-position (a , following the nomenclature in Fig. 2) dependent in the expression is t_f , which can be expressed as $t_f = 2a/V$ for a constant speed V . Note that for the experimental conditions evalu-

ated here, the expressions $\nu P t_f$ and λ are always between 0 and 1. The first few terms of the series expansion of an exponential is given in Eq. (11).

$$e^{-s} = 1 - s + \frac{s^2}{2!} - \frac{s^3}{3!} + \dots \quad (11)$$

For the case of a fractional value of s , the higher-order terms of the expression are alternating in sign and small in comparison to the first-order terms. Substituting the first-order terms from the exponential into the expression for c and simplifying yields,

$$c = [\lambda(1 - e^{-\nu P T})] + \left[(1 - \lambda) \frac{2\nu P}{V} \right] a \quad (12)$$

The terms in the square brackets of Eq. (12) are constants for any given test. While the analytical expressions were used in the model fittings, the above order-of-magnitude analysis describes the linear appearance of the model curves.

The monotonic rise in experimental curves in the low ($\mu < 0.05$) friction regime may be due to surface chemical or physical effects, in addition to coverage. These effects may include defect formation, defect annealing, and film formation, some of which have been identified in atomic-scale friction studies [19,20].

There are also some differences between the model curves and data. A striking difference is the trend in the data for the friction coefficient to be higher at both the beginning and end of a cycle at higher friction levels ($\mu > 0.05$). For these cases the model fails to describe the spatially resolved friction data. The friction coefficient near the turnaround points is higher than in the middle of the track, independent of direction of travel. Clearly, the friction coefficient is not proportional to surface coverage, as it was in the superlow friction regime.

This behavior in the high friction ($\mu > 0.05$) regime may be due to third bodies. Investigators have reported that transfer films are formed during sliding against DLC coatings in this friction regime [21,22] and with NFC coatings against non-NFC-coated counter-faces run in dry N_2 [23]. In contrast, transfer films have not been detected with NFC versus NFC coatings in the superlow friction regime [3,7]. The generation of transfer films at the higher friction coefficients indicates that gas-surface interactions promote detachment of material at the sliding interface. A gas could disrupt the passivating bonds at the nascent surface or produce surface films that detach intact. The likely gas culprit is H_2O , known to raise the friction coefficient of hydrogenated carbon coatings [8,24]. In situ tribometry has recently provided direct evidence that sliding against DLC coatings in humid air produces thicker transfer films and higher friction coefficients than in dry air [22]. Thus, moisture likely promotes particle detachment, which requires extra energy and raises the friction coefficient.

Finally, although the model does not describe the higher friction behavior, one of the fit parameters in the model suggests why the friction behavior changed. As seen in Fig. 1, the fraction removed for each pass ($1 - \lambda$) approaches 0 for the slower sliding speeds, when the friction coefficient rises the most. The model curves [17] and data for both the multiple sliding speeds and dwell experiments [7] leading to higher friction have been reexamined. Instead of looking at the fraction removed ($1 - \lambda$) as a function of sliding speed, the removal ratio λ as a function of steady-state friction coefficient was examined. No additional model fits were performed. Figure 6 shows that as the friction coefficient climbed toward 0.12 (λ approached a value of 1). Thus the model suggests that as the friction coefficient increases, it becomes harder to continuously remove the product of the gas-surface interaction by wiping. As continuous removal becomes less likely, removal could become discontinuous, for example, by coating fracture. However, surface analytical studies will be necessary to determine the actual physical changes that accompany the transition from the superlow to the higher friction (0.05 and up) regime.

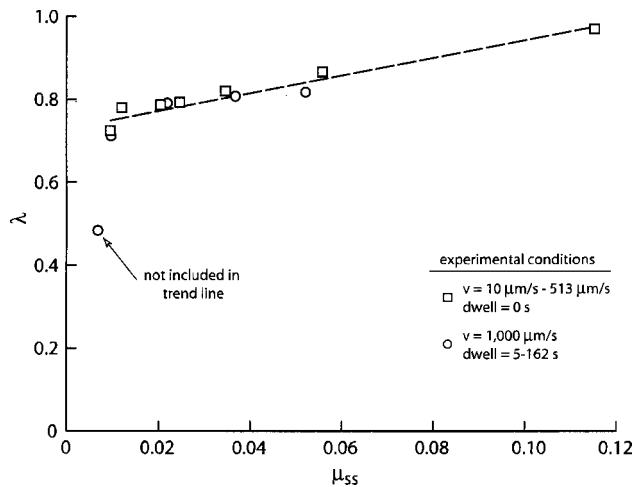


Fig. 6 A plot of the removal ratio λ versus the steady-state friction coefficient for experiments run under varying sliding speed and constant dwell, and experiments run at constant sliding speed and various dwell times.

Conclusions

A closed-form time- and position-dependent model for the coverage in a reciprocating pin-on-disk contact based on first-order gas kinetics has been developed. The model was first shown to be consistent with previous steady-state and time-dependent models based on the same underlying physics. Friction data, cycle averaged as well as position- and time-dependent, collected by Heimberg et al. [7] was compared to friction curves generated from the model; the latter used parameters from a midpoint model that was fit to the average data as presented in [17]. The position-dependent curves showed good agreement with data in the low friction range ($\mu < 0.05$), but deviated from the predicted linear behavior at higher friction coefficients, suggesting that the first-order kinetics models are not capturing all of the physics of the gas-surface interactions.

Acknowledgments

J. A. Heimberg was supported by an ASEE postdoctoral associateship. Funding for this project was provided by the Office of Naval Research and Department of Energy, Office of Energy Research. P. L. Dickrell was supported by a University of Florida Minority Fellowship.

References

[1] Erdemir, A., 2001, *Modern Tribology Handbook*, in *Mechanics and Materials Science Series*, B. Bhushan, Editor, CRC Press, Boca Raton, FL., pp. 787–825.

[2] Grill, A., 1999, "Diamond-Like carbon: State of the Art," *Diamond Relat. Mater.*, **8**, pp. 428–434.

[3] Erdemir, A., Eryilmaz, O. L., Nilufer, I. B., and Fenske, G. R., 2000, "Synthesis of Superlow-Friction Carbon Films From Highly Hydrogenated Methane Plasmas," *Surf. Coat. Technol.*, **133**, pp. 448–454.

[4] Erdemir, A., Fenske, G. R., Terry, J., and Wilbur, P., 1997, "Effect of Source Gas and Deposition Method on Friction and Wear Performance of Diamond-Like Carbon Films," *Surf. Coat. Technol.*, **94-5**, pp. 525–530.

[5] Erdemir, A., Eryilmaz, O. L., Nilufer, I. B., and Fenske, G. R., 2000, "Effect of Source Gas Chemistry on Tribological Performance of Diamond-Like Carbon Films," *Diamond Relat. Mater.*, **9**, pp. 632–637.

[6] Erdemir, A., 2001, "The Role of Hydrogen in Tribological Properties of Diamond-Like Carbon Films," *Surf. Coat. Technol.*, **146**, pp. 292–297.

[7] Heimberg, J. A., Wahl, K. J., Singer, I. L., and Erdemir, A., 2001, "Superlow Friction Behavior of Diamond-Like Carbon Coatings: Time and Speed Effects," *Appl. Phys. Lett.*, **78**, pp. 2449–2451.

[8] Andersson, J., Erck, R. A., and Erdemir, A., 2003, "Frictional Behavior of Diamond-Like Carbon Films in Vacuum and Under Varying Water Vapor Pressure," *Surf. Coat. Technol.*, **163-164**, pp. 535–540.

[9] Rowe, C. N., 1967, "A Relation Between Adhesive Wear and Heat of Adsorption for Vapor Lubrication of Graphite," *ASLE Trans.*, **10**, p. 10.

[10] Langmuir, I., 1916, "The Constitution and Fundamental Properties of Solids and Liquids," *J. Am. Chem. Soc.*, **38**, pp. 2221–2295.

[11] Bowden, F. P., and Rowe, G. W., 1957, "Lubrication With Molybdenum Disulphide Formed From the Gas Phase," *Engineer (London)*.

[12] Blanchet, T. A., Lauer, J. L., Liew, Y. F., Rhee, S. J., and Sawyer, W. G., 1994, "Solid Lubrication by Decomposition of Carbon-Monoxide and Other Gases," *Surf. Coat. Technol.*, **68**, pp. 446–452.

[13] Zaidi, H., Paulmier, D., and Lepage, J., 1990, "The Influence of the Environment on the Friction and Wear of Graphitic Carbons, Part 2. Gas Coverage of Wear Debris," *Appl. Surf. Sci.*, **44**, pp. 221–233.

[14] Cerofolini, G. F., and Re, N., 1995, "Extracting the Energy Distribution Functions of Heterogeneous Surfaces From Their Desorption Kinetics," *J. Colloid Interface Sci.*, **174**, pp. 428–440.

[15] Sawyer, W. G., and Blanchet, T. A., 2001, "Vapor-Phase Lubrication in Combined Rolling and Sliding Contacts: Modeling and Experimentation," *ASME J. Tribol.*, **123**, pp. 572–581.

[16] Blanchet, T. A., and Sawyer, W. G., 2001, "Differential Application of Wear Models to Fractional Thin Films," *Wear*, **251**, pp. 1003–1008.

[17] Dickrell, P. L., Sawyer, W. G., and Erdemir, A., 2004, "Fractional Coverage Model for the Adsorption and Removal of Gas Species and Application to Superlow Friction Diamond-Like Carbon," *ASME J. Tribol.*, **126**, in press.

[18] Sawyer, W. G., and Dickrell, P. L., 2004, "A Fractional Coverage Model for Gas-Surface Interaction in Reciprocating Sliding Contacts," *Wear*, **256**, pp. 73–80.

[19] Kopta, S., and Salmeron, M., 2000, "The Atomic Scale Origin of Wear on Mica and its Contribution to Friction," *J. Chem. Phys.*, **113**, pp. 8249–8252.

[20] Dickinson, J. T., Park, N.-S., Kim, M.-W., and Langford, S. C., 1997, "A Scanning Force Microscope Study of a Tribochemical System: Stress-Enhanced Dissolution," *Tribol. Lett.*, **3**, pp. 69–80.

[21] Donnet, C., 1998, "Recent Progress on the Tribology of Doped Diamond-Like and Carbon Alloy Coatings: A Review," *Surf. Coat. Technol.*, **101**, pp. 180–186.

[22] Scharf, T. W., and Singer, I. L., 2002, "Role of Third Bodies in Friction Behavior of Diamond-Like Nanocomposite Coatings Studied by In Situ Tribometry," *Tribol. Trans.*, **45**, pp. 363–371.

[23] Sanchez-Lopez, J. C., Erdemir, A., Donnet, C., and Rojas, T. C., 2003, "Friction-Induced Structural Transformations of Diamond-Like Carbon Coatings Under Various Atmospheres," *Surf. Coat. Technol.*, **163**, pp. 444–450.

[24] Donnet, C., Le Mogne, T., Ponsoonnet, L., Belin, M., Grill, A., Patel, V., and Jahnes, C., 1998, "The Respective Role of Oxygen and Water Vapor on the Tribology of Hydrogenated Diamond-Like Carbon Coatings," *Tribol. Lett.*, **4**, pp. 259–265.